Title: Estimating Floating Macroplastic Flux in the Santa Ana River, California

Authors: Win Cowger[*1,2], Andrew Gray[1], Stanley Brownlee[1], Hannah Hapich[1], Ashok Deshpande[3], Kryss Waldschläger[4]

*Corresponding author

Affiliations:

1. University of California, Riverside, 900 University Ave, Riverside, CA 92521
2. Moore Institute for Plastic Pollution Research, 160 N. Marina Dr. Long Beach, CA 90803
3. NOAA Fisheries, 74 Magruder Road, Sandy Hook, New Jersey
4. Hydrology and Quantitative Water Management Group, Wageningen University and Research, Wageningen, The Netherlands

Abstract

1. Study Region

The middle reach of the Santa Ana River, a small coastal urban catchment in Southern California, USA experiences a Mediterranean climate and lowflows dominated by wastewater effluent.

2. Study Focus

River macroplastic flux can inform watershed management of plastic pollution. However, continuous macroplastic monitoring is not currently possible, so concentrations must be predicted during unobserved periods. We monitored macroplastic concentration in the Santa Ana River and attempted to improve our estimation of macroplastic flux using strategies commonly employed in studying mineral sediment flux.

3. New Hydrological Insights for the Region

Floating macroplastic particle size distributions were statistically equivalent between lowflow (when only the channel provides macroplastic to the river) and stormflow samples (when urban runoff also contributes macroplastic to the river) – evidence that channel processes controlled macroplastic particle size distribution. Concentrations fell during the falling limb of one hydrograph and rose during the rising limb of another hydrograph. A generalized additive model (GAM) revealed that macroplastic concentration increased in response to small increases in discharge but decreased for the largest discharges. The annual mass flux of floating macroplastic was (27.4, 2.8-84.8 tonnes^{1}yr^{-1}) or (18.2, 2.9-222.2 tonnes^{1}yr^{-1}) as predicted using mean concentration or the GAM, respectively. With little data, the mean concentration approach may be appropriate but likely underestimates uncertainty – the reduction of which will require extensive monitoring.

Graphical Abstract

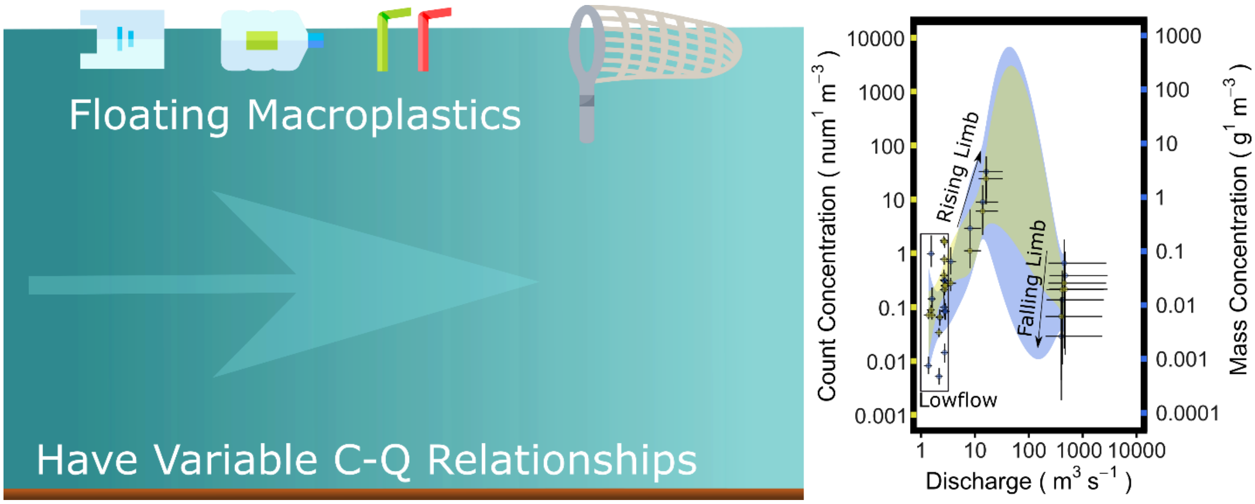

Abbreviations

FTIR: Fourier transformed infrared spectroscopy

Pyrolysis GCMS: Pyrolysis gas chromatography mass spectrometry

USGS: United States Geological Survey

ATR: attenuated total reflectance

Keywords

Plastic Pollution, Concentration-discharge Relationships, Anthropogenic Litter, Transport, Pathways, Hysteresis

1.0 Introduction

Rivers are highly contaminated by plastic pollution and are the major conveyance of plastic from land to the ocean (Lebreton et al., 2017). River plastic flux (plastic quantity discharged per unit time) is a key variable in interpreting the magnitude of plastic transport to downriver ecosystems, the pollution at the study location, and changes in the magnitude of upriver plastic sources (Schmidt et al., 2017; Watkins et al., 2019). Macroplastic (> 5 mm) particles are known to make up most of the mass of plastic in the environment and break down to form many more abundant microplastics (particles < 5 mm) (L. Lebreton, B. Slat, F. Ferrari, B. Sainte-Rose, J. Aitken, R. Marthouse, S. Hajbane, S. Cunsolo, A. Schwarz, A. Levivier, K. Noble, P. Debeljak, H. Maral, R. Schoeneich-Argent, R. Brambini & J. Reisser, 2018; Moore et al., 2011). Rigorous estimates of river macroplastic flux are critical for addressing the global crisis of plastic pollution (Bai et al., 2021) but has been much less studied than microplastic flux (van Emmerik, 2021).

River macroplastic flux is typically quantified by multiplying river discharge (m^3s^{-1}) by macroplastic concentrations (count or $mass^1m^{-3}$). Continuous river stage (m) measurements are available in many locations within the United States and are periodically calibrated to discharge (m^3s^{-1}), velocity (m^1s^{-1}), depth (m), and other river flow characteristics by the United States Geological Survey (USGS). However, no methods to continuously monitor river macroplastic concentration are currently in use. One needs to make predictions about unobserved macroplastic concentrations to quantify macroplastic flux.

Mineral sediment transport has a long history of research and can inform strategies for studying plastic transport (Waldschläger et al., 2022). Unobserved concentrations of fluvial particulate matter are often predicted using discharge regime, hydrograph hysteresis, and rating curves fit to river discharge (Gray, 2018; Rose et al., 2018; Walling, 1977). Changes in discharge reflect combined changes in the supply and transport of water to the monitoring stations and affect changes in the river's transport properties (e.g., turbulence, velocity, depth). The ratio between the flux of water and the flux of particulates at any moment is reflected in the average concentration of the particulate in the flow. Multiple orders of magnitude of variability around the concentration-discharge rating curves are typical, particularly in the small mountainous rivers characteristic of coastal California (Gray, 2018). This variability is due in part to stochastic processes like storm sequence (East et al., 2018), spatio-temporal characteristics (Aguilera and Melack, 2018), and antecedent watershed conditions (Fisher et al., 2021; Gray et al., 2015; Warrick and Rubin, 2007), which can cause changes in the processes controlling water and sediment delivery and routing (Gray et al., 2014). Temporal structure to this variability can manifest in concentration-discharge relationships from hydrograph hysteresis (Williams and Others, 1989)(i.e., different rising vs falling limb concentration-discharge relationships) to interdecadal scale trends (Gray, 2018; Warrick et al., 2013). A "first flush" event is common for sediment, whereby high concentrations are flushed during the first large storm event of the year (Sansalone John J. and Cristina Chad M., 2004). The particle size distribution of the suspended load may shift with hydrologic mode (stormflow, lowflow) and can be diagnostic of sources and transport pathways of mineral sediment (Li Yingxia et al., 2005; Slattery and Burt, 1997). Investigation of temporal patterns in concentration-discharge relationships can provide insight into transport and supply processes and be used to refine flux estimation (Farnsworth and Milliman, 2003; Gray et al., 2014; Warrick and Rubin, 2007). We build from these foundations of fluvial sediment concentration-discharge relationships to advance the fundamentals of macroplastic concentration-discharge relationships.

Early research on plastic pollution suggested that macroplastic concentration-discharge relationships should be considered in estimating plastic discharge from rivers. River macroplastic particle count to mass ratios were assumed constant in literature (Van Emmerik et al., 2019) despite changes in hydrological mode, suggesting stable particle size distributions but changes in macroplastic particle size distributions have not been tested. Our first aim was to test the hypothesis that macroplastic particle size distributions were stable regardless of hydrologic mode. Stormflow events have been observed to increase macroplastic concentration compared to lowflow (van Emmerik et al., 2019) but macroplastic concentration discharge hysteresis has not been tested in the literature. Our second objective was to test whether hysteresis or storm timing may play a role in these event to seasonal scale concentration-discharge relationships. Rating curves have been observed between plastic concentration and discharge as decreasing (van Emmerik et al., 2018; Watkins et al., 2019), increasing (Moore et al., 2011), stable (Wagner et al., 2019), and nonmonotonic (Haberstroh et al., 2021), reflecting a similar diversity of rating curves that can be watershed or even event specific as seen in other particulate transport studies. This underscores the need for more regional studies on plastic concentration discharge rating curves and resultant flux estimation. Our third goal was to assess the macroplastic concentration-discharge rating relationship in the Santa Ana River, and evaluate its use to estimate the annual flux of macroplastic at our study location during the study year. In total, these objectives serve to inform science about transport processes of macroplastic in rivers and inform society about how to best manage macroplastic pollution.

2.0 Study Location

The Santa Ana River drains a small mountainous watershed (total area: 6900 km^2, area at survey location: 2341 km^2) and experiences a hot dry summer Mediterranean climate regime, with > 90% of its 61 cm of average annual precipitation occurring between October-April (Figure 1). The study location on the Santa Ana River was monitored where the river crosses the Van Buren Bridge in Riverside, CA, which is 1.8 km downriver from USGS gage 11066460. The bridge above the stream was used during stormflow sampling and sampling was conducted in the stream during lowflow. The main stem of the Santa Ana River in the vicinity of sample collection displays two major hydrologic regimes: low magnitude (mean daily discharge (USGS codes: par 60, stat 00003) = 1.8 $m^3\ s^{-1}$) flows supported entirely by wastewater discharge, and flashy storm flows (mean daily discharge: 14.0 $m^3\ s^{-1}$; and 2 year recurrence interval daily flow of 64.3 $m^3\ s^{-1}$) (Figure S1). For most of the time, the middle reach of the Santa Ana is a losing river with discharge decreasing downriver unless fed by a stormflow event or at wastewater input points. Naturally the study location would have no or little flow without wastewater input for most of the year. Wastewater systems are separated from stormwater in the watershed, so the wastewater treatment plant does not treat stormwater. The sampled reach is low gradient (slope = 0.004), sandy fine gravel bedded, and includes a vegetated riparian corridor that persists between flood control levees. These characteristics are typical of interior trunk streams in Southern California and thus the study location is a suitable representative of streams draining highly urbanized watersheds in this region.

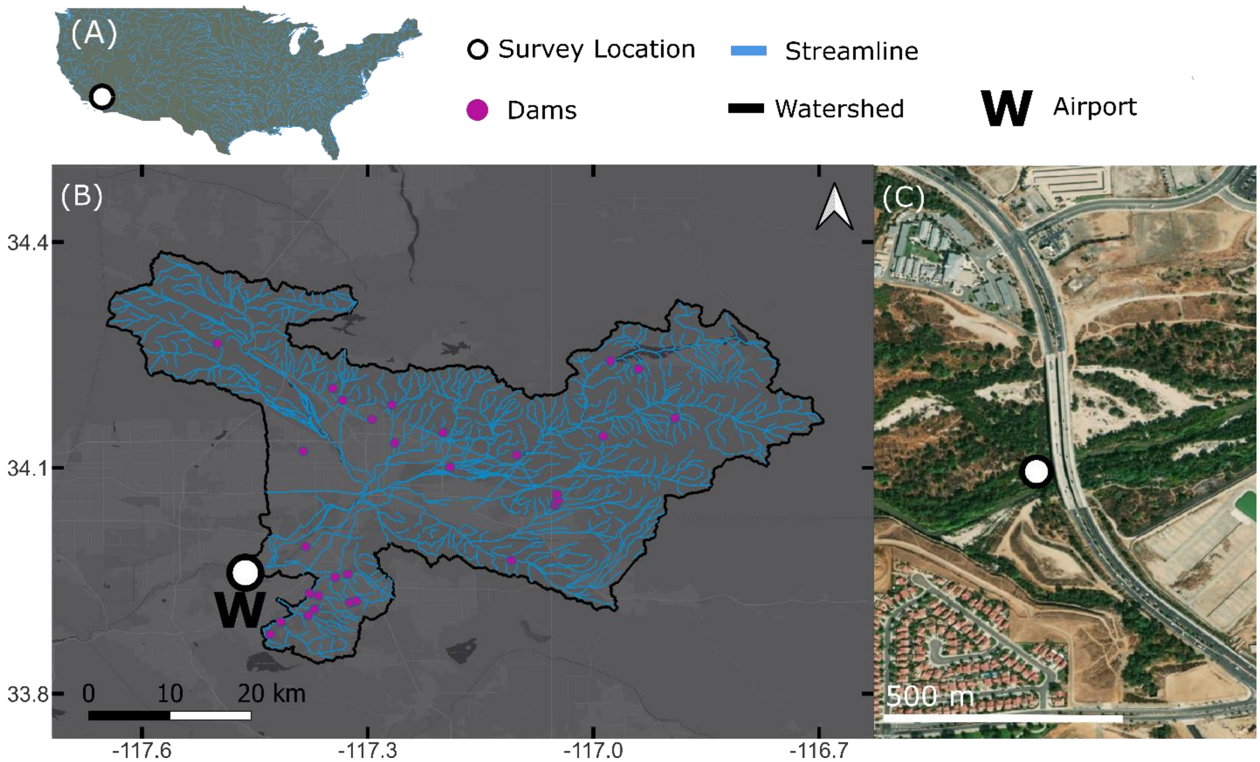

Figure 1: The study (A), watershed (B), and survey location (C) of this study. The white dot is the location where the samples were taken. (A) shows the watershed location in the United States. In (B) the basemap is the ESRI Dark Basemap where urban areas and roads are in lighter gray and darker areas are natural lands. Stream centerlines are added from the National Hydrography Dataset in blue (USGS, 2019). The Watershed boundary was delineated using Streamstats from the USGS (USGS, 2016a). The National Inventory of Dam ("National Inventory of Dams," 2018) locations were plotted as pink dots. (C) Satellite imagery of the study reach is shown from Google Earth, and the survey location is downstream of the Van Buren Bridge in Riverside, CA.

Pathways and fate of macroplastic at the study reach depend on water and trash management within the watershed and channel. A large amount of accumulated trash exists as standing stock within the channel riparian area (Moore et al., 2016), but there have not been previous studies on trash flux through the Santa Ana River. Potential sources of macroplastic to the channel are suspected to be runoff from upstream urban areas, direct dumping within the river, and unmanaged waste from populations of unhoused people that live within the riparian area (Cowger et al., 2019; Moore et al., 2016). Urban runoff is mitigated through street sweeping and trash capture devices in storm drains (Cowger et al., 2022; Riverside City, 2021; Riverside County, 2010). However, to our knowledge, there are no systematic mitigation measures for removing trash within the channel. The watershed upriver of the sample location includes 31% developed land use. Immediately adjacent and upriver of the sample location is the major metropolitan area of the Inland Empire, including Riverside and San Bernardino cities. Wastewater facilities that input to the Santa Ana have secondary or tertiary treatment before the wastewater is transferred to the channel. They are suspected to be a negligible source of macroplastic due to the filtration used during the treatment processes. Near the watershed's headwaters are mountains with primarily rural populations, but these sections are generally disconnected from the sampling reach due to dams at the foothills of many mountain tributaries and the losing nature of the river channel most of the year. Downriver of the study location is the Prado Dam, which likely prevents most trash flux from the study reach from reaching the ocean due to cleanup activities at the dam.

3.0 Methods

Methodological descriptions were written to ensure reproducibility and interpretability of the study methodology following best practices for microplastics research, recognizing that there were no current recommendations for macroplastic (Cowger et al., 2020).

3.1 Field Measurements

3.1.1 Macroplastic measurements

River macroplastic samples were collected in the Santa Ana River from the downriver side of the Van Buren bridge in Riverside, California (Figure 2, 3, & 4). A steel box trawl (designed by Dr. Marcus Eriksen of 5 Gyres) with a square 0.16 m^2 intake and 5 mm polyester rope net was lowered from a bridge to the thalweg of the river using a portable crane (USGS Type A Crane with 3 Wheel Truck) attached to the trawl with rope and a boat shackle. As the thalweg moved locations, we followed it with the sampler. On average, half of the net was submerged if the net was not resting on the river bed. To sample lowflows, we waded into the river and set the net in the thalweg of the channel on the river bed. The total number of samples collected was limited to 20 over the course of 5 sampling events (Figure 4) due to the highly episodic and fast-moving river flow in Southern California. Our goal was to sample multiple time points during all 2018 water year (October 1st 2018 - September 30th 2019) stormflow events and during three lowflow events. However, stormflow in Southern California is highly episodic, making it challenging to collect stormwater samples since three field technicians were required to be available during a 24 hour window of potential operations with only 1-2 day notice. Additionally, Southern California stormflow can be fast-moving (> 3 m/s), forcing sampling to stop when conditions become too dangerous due to large objects (e.g., trees, dumpsters, tires, beds) flowing down the river or the sampling equipment violently jumping out of the water. Because of these issues, we could only sample during 2 of 5 stormflows in water year 2018.

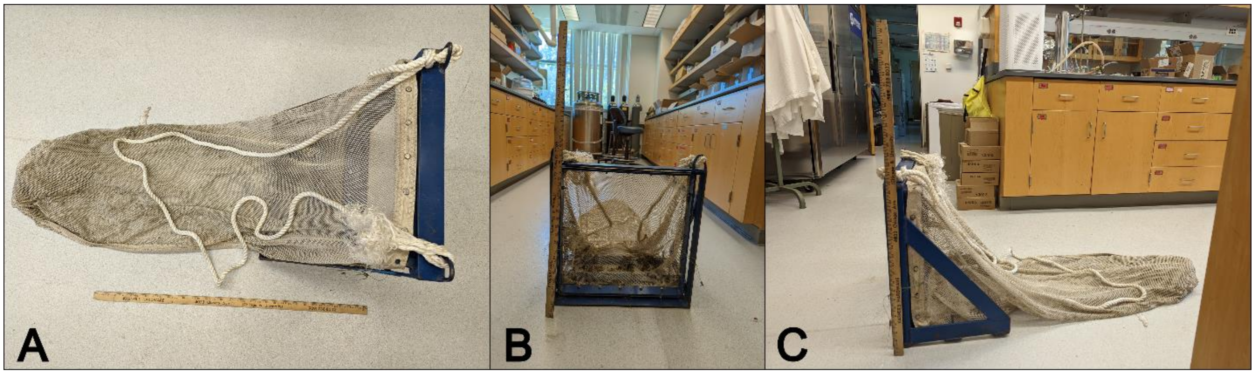

Figure 2: Sample collection net with a yard stick (0.91 m) for scale. A) Top view of the net. B) front view into the intake of the net. The net has a 400 mm square aperture and a 5 mm mesh. C) side view of the net.

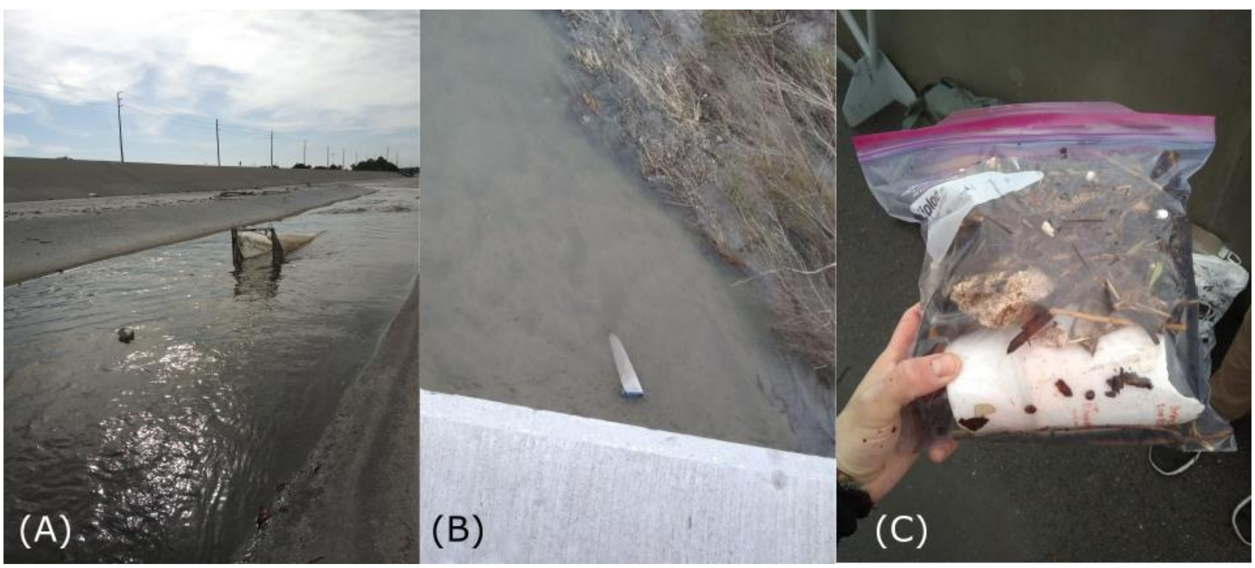

Figure 3: A) net deployment from inside a channel, B) net deployment from a bridge, C) an example of a sample that will be visually sorted for macroplastic.

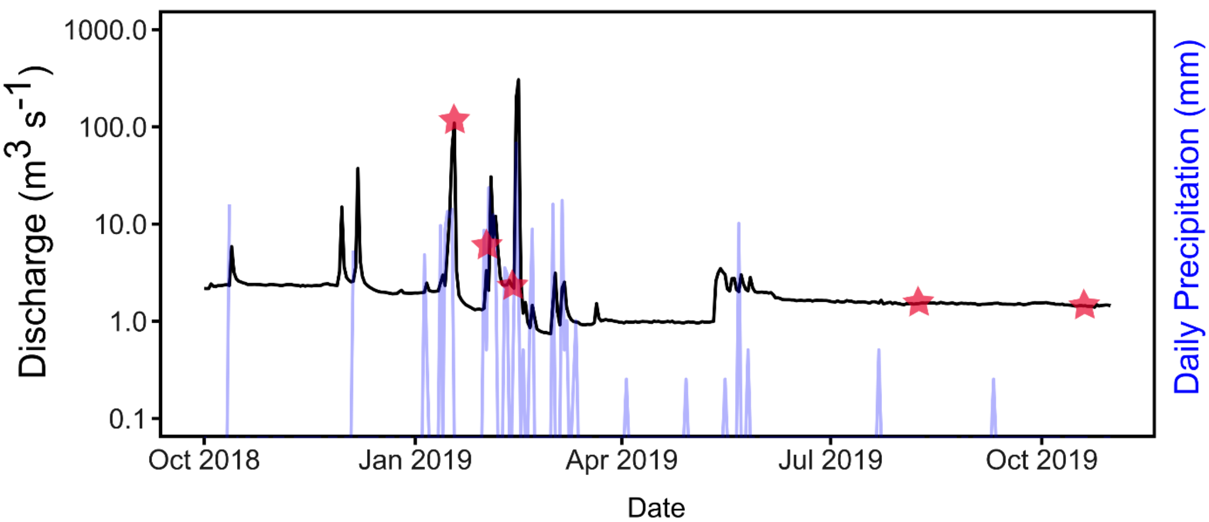

Figure 4: The hydrograph (mean daily average cubic meters per second) from October 1st 2018 to October 30th 2019. Y axis (discharge and daily precipitation) is in log 10 scale while x axis is in days with quarterly tickmarks. Red stars mark the days when samples were acquired. Hyetograph in blue (daily precipitation in mm) is overlayed but uses the same values as discharge.

3.1.2 Hydrologic Measurements

All river hydrologic data were obtained from the USGS river gage 11066460 located 1.8 km upriver from the macroplastic sampling location (USGS, 2016b). The river gage was inspected. Flow conditions and morphological characteristics were similar to the survey location. Continuous stage data (15 min) (gage height) (USGS parameter 65) were acquired along with measurements of channel discharge (USGS parameter 61), river velocity (USGS parameter 55), channel cross-sectional area (USGS parameter 82632), and channel width (USGS parameter 4) from 2018-01-10 to 2020-04-21. The channel cross-section shape was generally rectangular at both the survey and gage locations. The river cross-sectional area was divided by width to estimate the average river depth. USGS measurements were used to create rating curves using linear regression on $\log_{10}$ transformed stage and measured variables. Log_{10} transformation bias ($\log_{10}$ correction) was corrected using the approach of Ferguson (Ferguson, 1986). The adjusted r squared (adjRSQ) value was derived for each regression in R to describe the amount of variability around the regression. The discharge rating curve was ($\log_{10}$(discharge) = 5.1 * $\log_{10}$(gage height) – 1.49, adjRSQ = 0.76, $\log_{10}$ correction = 1.09, p value = 10^{-16}). The velocity rating curve was ($\log_{10}$(velocity) = 1.24 * $\log_{10}$(gage height) – 0.58, adjRSQ = 0.44, $\log_{10}$ correction = 1.02, p value = 10^{-9}). The depth rating curve was ($\log_{10}$(depth) = 2.67 * $\log_{10}$(gage height) – 2.03, adjRSQ = 0.73, $\log_{10}$ correction = 1.03, p value = 10^{-16}). Uncertainty in USGS rating curves was propagated using bootstrap simulation (resampling with replacement, n = 10,000) of the USGS measurements. River slope was estimated using the 1/9th arc-second digital elevation model from the National Elevation Dataset (USGS, 2017) and Google Earth. River shear velocity (u_*) was estimated as:

$$u_* = \sqrt{ghs} \qquad \text{equation 1}$$

where (h) is the average river depth, (g) is the acceleration due to gravity, and (s) is the river slope (de Leeuw et al., 2020). Daily precipitation (Figure 4) was downloaded from Midwestern Regional Climate Center's cli-MATE application (Midwestern Regional Climate Center, 2021) for the KRAL airport weather station near the sample location (Figure 1).

3.2 Plastic particle characterization

Macroplastic particles were visually sorted from the samples and photographed with a scale in the image (Figure 5A). We used Image J (Schindelin et al., 2012) to quantify particle projected area (Figure 5B) for each particle using Image J's color thresholding, manual tracing, and particle size analysis routines (Figures 5A & 5B). Particle projected area is the area of the image which contains the particle. Particle projected area contains no information about the third dimension (the height) of the particles. We did not account for the third dimension of the particles in this analysis instead we standardized the smallest dimension to be out of view by laying the largest dimensions facing upward to the camera view, and in our opinion, the advantages of the high throughput reproducible approach outweighed the loss of measuring the third dimension. Small artifact “particles” visible at the fringes of particles (Figure 5B) were removed by restricting the minimum particle size to 1 mm^2. Nominal particle size was estimated as the square root of the particle projected area. Particles are well separated by this technique and outlined precisely. Suspected error in particle size measurement using this technique is less than 1 mm.

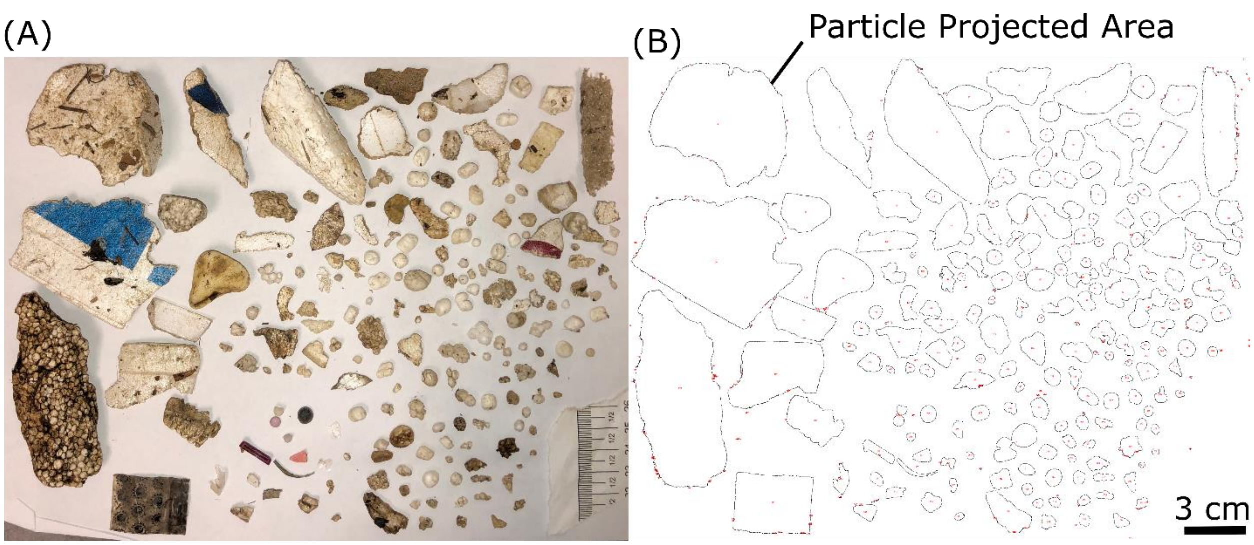

Figure 5: (A) Plastic particles extracted from samples in the Santa Ana River. (B) An outline image showing the traced projected surface area of each plastic particle. Scale in (B) is for both images as they have the same exact scale.

All suspected plastic particles were subjected to a sink-swim test by placing them in fresh water from the lab de-ionized water faucet, agitating the particle until no surface bubbles were visible, and assessing if the particle floated or sank. All particles were labeled as settling or buoyant.

A subset of 88 out of 944 particle identities were validated using fourier-transformed infrared (FTIR) spectroscopy and 30 particles with pyrolysis gas chromatography mass spectrometry (PY-GCMS). The smallest particles of the samples were chosen for validation because they were the most likely to be misidentified (Kroon et al., 2018). For FTIR, a Thermo Nicolet 6700 attenuated total reflectance (ATR) FTIR was used at 4/cm spectral resolution with daily background recording for the spectral range from 400-4000 wavenumbers (1/cm). Spectral analysis was done in Open Specy (Cowger et al., 2021b) with smoothing conducted with a Savitzky-Golay filter with a window size of 12 points and a 3rd order polynomial, baseline correction conducted with the imodpolyfit routine using an 8th order polynomial, and a min-max normalization before identification. Identification was conducted using Pearson correlation and a 0.5 uncertainty threshold using the entire spectral range. In Pyrolysis GCMS, the plastic sample was pyrolyzed in a quartz tube at a temperature of 750 C by using the CDS-2000 Pyroprobe. The Agilent 6890N GC used a CDS-1500 Valved GC Interface held at 320 C and the hydrogen gas flow rate was 1.2

ml min^{-1} in constant flow mode. The column characteristics were DB-5 (0.25 mm OD x 60 m L; 0.25 µ film thickness) fused-silica capillary column. The CDS-1500 GC Interface valve was closed after one min. The column oven temperature was initially held at 45°C for 2 min and then ramped to 320°C at 20°C min^{-1} rate. The column oven was held at 320°C for 19 min resulting in a total run time of 34.75 min. The MS electron Multiplier (EM) auto-tune voltage was adjusted by 200V above the auto-tune voltage. Data acquisition was performed in full-scan mode from 29-600 amu by using the Agilent ChemStation Software. The Injector and the Mass Spectrometer Transfer Line Heater were maintained at 320°C. The mass spectrometer Quadruple and Source temperatures were held at 150°C and 230°C.

Results from spectral analysis demonstrated highly accurate visual differentiation of plastic from the samples. Pyrolysis GCMS identified 28 of the 30 particles as plastic, 1 particle as non-plastic, and 1 particle as unknown. FTIR identified 67 as plastic and 3 particles as non-plastics, with 18 that could not be identified. Pyrolysis GCMS utilized a two-tier approach comprising of peak fingerprinting and mass spectra of marker peaks. The two-tier confirmation approach provided increased confidence in the quality of the polymer identification data. Pyrolysis GCMS was used to further validate our FTIR analysis by comparing 8 particles with both techniques resulting in 6 particles had the same identity with both techniques, 1 particle being identified as a different polymer (polyethylene instead of polypropylene), and 1 particle not being able to be identified by either Pyrolysis or FTIR (SI).

Thirteen macroplastic particles from these samples with rising velocities (positively buoyant) were randomly chosen to measure rising velocities and reported on in another publication (Waldschläger et al., 2020). They were composed of expanded polystyrene, polyethylene, and polypropylene, and had powers roundness ranges from 2.2-5.9, Corey shape factor from 0.07-0.88, dimensionless diameter of 2.5-30.81, and rising velocities ranging from 0.221-1.69 m/s.

3.3 Estimating macroplastic concentrations and uncertainties

Three types of macroplastic concentrations (count^{1}, projected area^{1}, or mass^{1} meter^{-3}) were estimated along with their uncertainties. All three calculations required an estimate of sample water volume. Submerged net depth was set to 0.2 m (half of the net height) or the average river depth, whichever was smaller. We multiplied the depth of the submerged net by the width of the net (0.4 m) to get the submerged cross-section of the net. Uncertainty of submerged depth was incorporated by simulation for each sample using a uniform probability density function from 0.1 – 0.3 m. The average river velocity from the USGS rating curve (linear model on $\log_{10}$ transformed data with $\log_{10}$ bias correction) was multiplied by the submerged cross-sectional area and the sample duration to quantify the sample's water volume. River velocity rating curve uncertainties were incorporated into sample size uncertainty using bootstrap simulation of the model fit (resampling with replacement, n = 10,000).

We removed a subset of macroplastic particles from our observations that would have biased our results: settling particles and particles < 5 mm. Microplastic particles can be transported in surface load, wash load, bed load, and rising or settling suspended load (Cowger et al., 2021a). Surface sampling (conducted in this study) best measures surface load because bed load and settling suspended load particles will preferentially pass beneath the sampler uncollected. Therefore, we limited this study to particles with a high likelihood of being in surface load transport (positively buoyant particles). We compared the freshwater settling plastics with the positively buoyant particles by size and count for all samples (Figure 6). We found that positively buoyant plastics were the most common plastic-type in the samples (98 %). The spectral analysis also corroborated that the vast majority of plastic materials were polyethylene, polypropylene, and polystyrene (expanded foam), which are more likely to float in water (Muthuvairavasamy, 2022). We removed the 17 settling particles from further analysis. We also noticed that the particle size distribution decreased in abundance around 5 mm in size, which corresponded to the net's mesh size. All particles smaller than 5 mm were removed from further analysis. We permuted all estimated shear velocities and all observed rising velocities of the particles to derive Rouse numbers.

$$P = \frac{w_s}{\beta k u_*} \qquad \text{equation 2}$$

The Rouse number (P) is derived by dividing the particle settling velocity ws by the multiple of β a parameter that adjusts the assumption of parabolic eddy diffusivity (set to 1), k the von Karmen constant (set to 0.4), and u_* the shear velocity. The largest mean Rouse number was -2.5, suggesting that most particles observed were in surface load transport (Cowger et al., 2021a). Therefore, we assumed that all particles in this study were transported at the surface of the water column. We used the depth-integrated average concentration estimate introduced by (Lebreton et al., 2017) and (Cowger et al., 2021a) to have a small bias for surface sampling particles in surface transport.

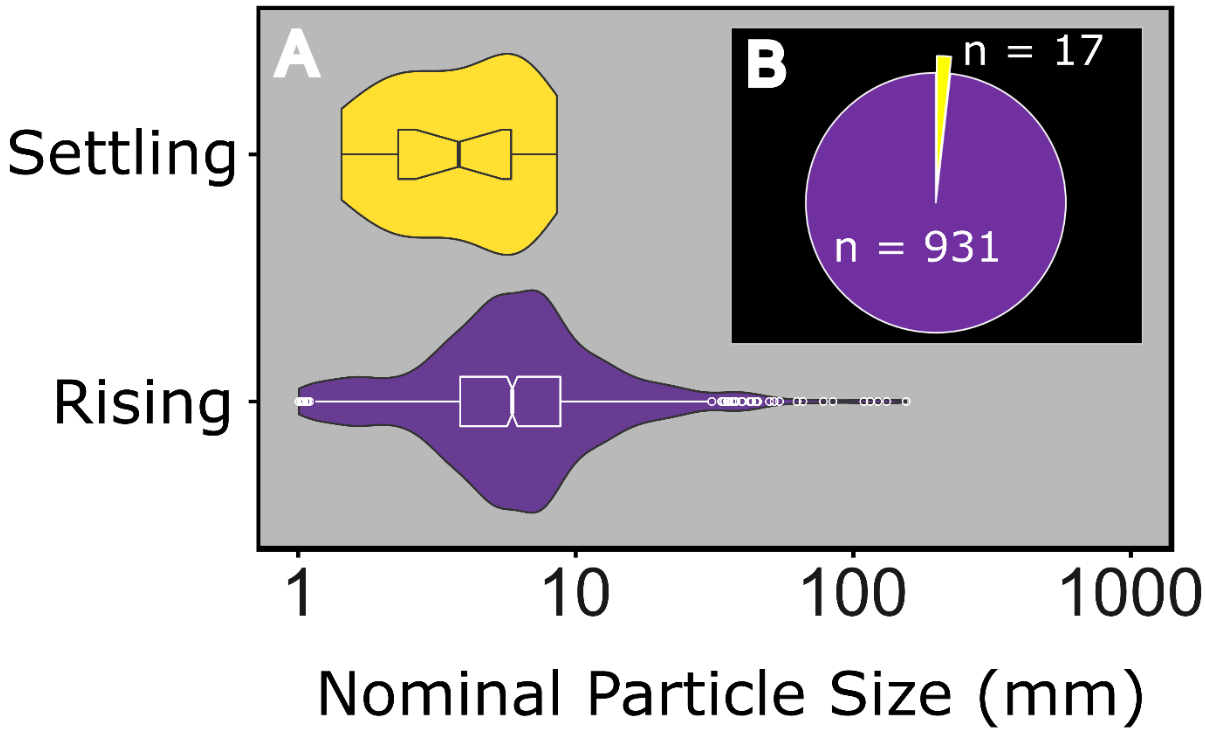

Figure 6: A) Nominal particle size distributions (the square root of the projected surface area) for settling and rising particles in this study. Violin plots are centered with notched box plots within (95% confidence interval). Violin plots are a smoothed and symetric representation of the probability density function of the particle size distributions. Dots show points beyond 1.5 times the interquartile range. Particle abundances dropped off for particles smaller than 5 mm in nominal particle size (the size of the mesh on the net). B) Pie chart showing the number of particles found with settling velocities (yellow) and rising velocities (purple). There were many more particles with rising velocities (931) than with settling velocities (17).

Count, area, and mass concentrations were calculated by dividing the abundance by sample volume. Count concentration was calculated by counting the number of particles in the sample (after removing bias-causing particles described in 3.2) and dividing it by the total sample water volume. Count uncertainty (due to fragmentation from handling, missing particles, and inadequate sampling of particle counts) estimated as up to ±10% of the sample count and was propagated using a uniform probability density function from 0 – 10%. Area concentration (mm^2m^{-3}) was calculated by summing the projected surface area from all particles in the samples and dividing it by the sample volume. Area uncertainty was estimated in the same way as count uncertainty. We measured the mass of 124 of the suspected macroplastic particles imaged for particle size measurement. We derived a linear regression on $\log_{10}$ transformed data between the particle projected area and the mass of the particle ($\log_{10}$(particle mass (g)) = 1.13 * $\log_{10}$(particle area (mm^2) – 4, adjRSQ = 0.63, $\log_{10}$ correction = 1.36, p value < 10^{-16}) (Figure 7) and corrected for $\log_{10}$ transformation bias (Ferguson, 1986). Then we used the regression to estimate the mass of all particles from our samples. Mass concentrations (g^1m^{-3}) were computed by dividing the total mass of macroplastic by the sample volume. Mass uncertainty was computed in the same way as area and count uncertainties.

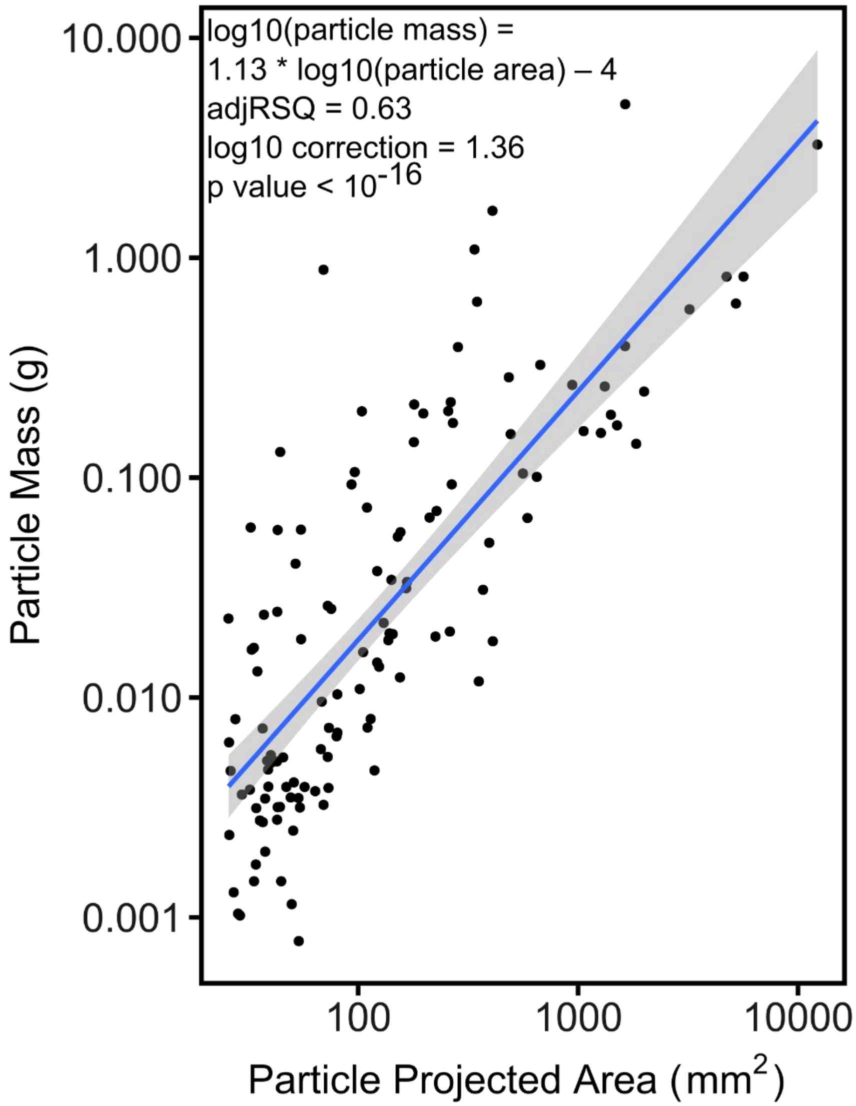

Figure 7: Each black dot is a particle with a particle mass (g) (y axis) and projected area (mm^2) (x axis). Axes are log10 transformed. The blue line represents the linear fit on log_{10} transformed data. The gray area is the 95% confidence interval around the central tendancy of the fit. The regression equation, adjusted r squared, log 10 correction value, and p value are printed in the top lefthand corner of the plot.

3.4 Lowflow and stormflow particle size distribution

Stormflow samples were visually separated from lowflow samples by using the hydrograph's slope change inflection points. All particles from stormflow and lowflow samples were pooled to make two particle size distributions (empirical cumulative density function). We used the two-sample Kolmogorov-Smirnov test to assess the null hypothesis that the particle size distributions of stormflow and lowflow were from the same distribution.

3.5 Hydrograph hysteresis and storm timing

We tested for hydrograph hysteresis and storm timing effects on the macroplastic concentration-discharge relationship. To assess hysteresis, we connected the sample concentration-discharge values for each sampling day with a line, and drew an arrow indicating the relationship's direction through time. We assessed the relationship between the hydrograph domain (rising limb, falling limb) during each stormflow sampling event and the hysteresis. Stormflow periods were determined using the description in 3.5. The rising limb was separated from the falling limb by assessing whether the discharge increased (rising limb) or decreased (falling limb) at the sample time. Storm timing was assessed by plotting the 2018 water year discharge time series (October 1st 2018 - September 30th 2019) plus the month of October 2019 to include the final sample in the study. We described the likely relationships between the timing and magnitude of the stormflows and the concentration-discharge relationships observed. Since only two stormflow events were sampled, we did not compute statistics on these trends and used them as a heuristic tool to identify future areas of study.

3.6 Macroplastic concentration-discharge rating curve

We assessed the concentration-discharge rating curve for count and mass concentrations using generalized additive modeling with a smoothing spline. This model allows the variety of concentration-discharge rating curves (non-monotonic and monotonic) to be fit (Gray, 2018). We tested the assumption of normality for $\log_{10}$ transformed concentrations using the Shapiro-Wilk test, and decided that we would use the assumption of normality for the model (count concentration, W = 0.92, p value = 0.08 | mass concentration, W = 0.97, p value = 0.82). We fit the generalized additive model to $\log_{10}$ transformed macroplastic concentrations and discharge using a smoothing spline (k=7). We assessed our confidence in the model fit using the p-value (alpha = 0.05), and deviance explained.

3.7 Estimating annual mass flux

We tested two commonly employed techniques, mean concentration extrapolation and the concentration-discharge rating curve, for estimating the mass flux of macroplastic in water year 2018 at the site to assess the importance of uncertainties and concentration-discharge rating curves (Gray, 2018). The continuous discharge of the water year 2018 was estimated from the continuous stage using a rating curve (section 3.1.2). Using mean concentration extrapolation, we estimated mass flux by assuming steady mean concentration using the mean mass concentration observed from our dataset. Total discharge for the water year 2018 was multiplied by the mean mass concentration to predict the annual flux. Using the generalized additive model rating curve, we predicted concentration for every discharge on record (15 min interval discharge). Mass flux was computed for every 15 min discharge interval and summed for the entire year. For both methods, confidence intervals were derived using 10,000 simulations with bootstrapped datasets for all data and models (resampling with replacement).

3.7 Statistical Analysis

All statistical tests and plots were written in reproducible R code, starting from raw data and ending with the outputs. The packages dataRetrieval (De Cicco et al., 2021), dplyr (Wickham et al., 2020), ggplot2 (Wickham, 2016), mgcv (Wood, 2011), readxl (Wickham and Bryan, 2019), data.table (Dowle and Srinivasan, 2020), stringr (Wickham, 2019), viridis (Garnier, 2018), tidyr (Wickham and Henry, 2020), MASS (Venables and Ripley, 2002), and matrixStats (Bengtsson, 2021) were used in the code.

4.0 Results and discussion

4.1 Lowflow and stormflow particle size distribution

We tested for differences in the macroplastic particle size distributions during lowflow and stormflow. Smaller size classes were exponentially more abundant than larger sizes for both hydrologic regimes (Figure 8). A similar particle size distribution has been observed for microplastic particles (Kooi and Koelmans, 2019). The maximum distance between the two cumulative distribution functions was 0.080 (p-value = 0.66). The particle size distributions of macroplastic particles in stormflow and lowflow samples were statistically indistinguishable. There was also high goodness of fit (adjRSQ = 0.63) between particle mass and particle projected area observed in our study (Figure 7). (van Emmerik et al., 2018) assumed a constant count- mass ratio for macroplastic floating in rivers, which would be suspected if the particle size distribution were also stable there. Assuming this stability continues in the future and is widespread, mean count-mass-area conversion ratios (common conversions in the field) should be constant regardless of discharge at a given site. Future work should compare our particle size distribution to distributions elsewhere to look for spatial variability.

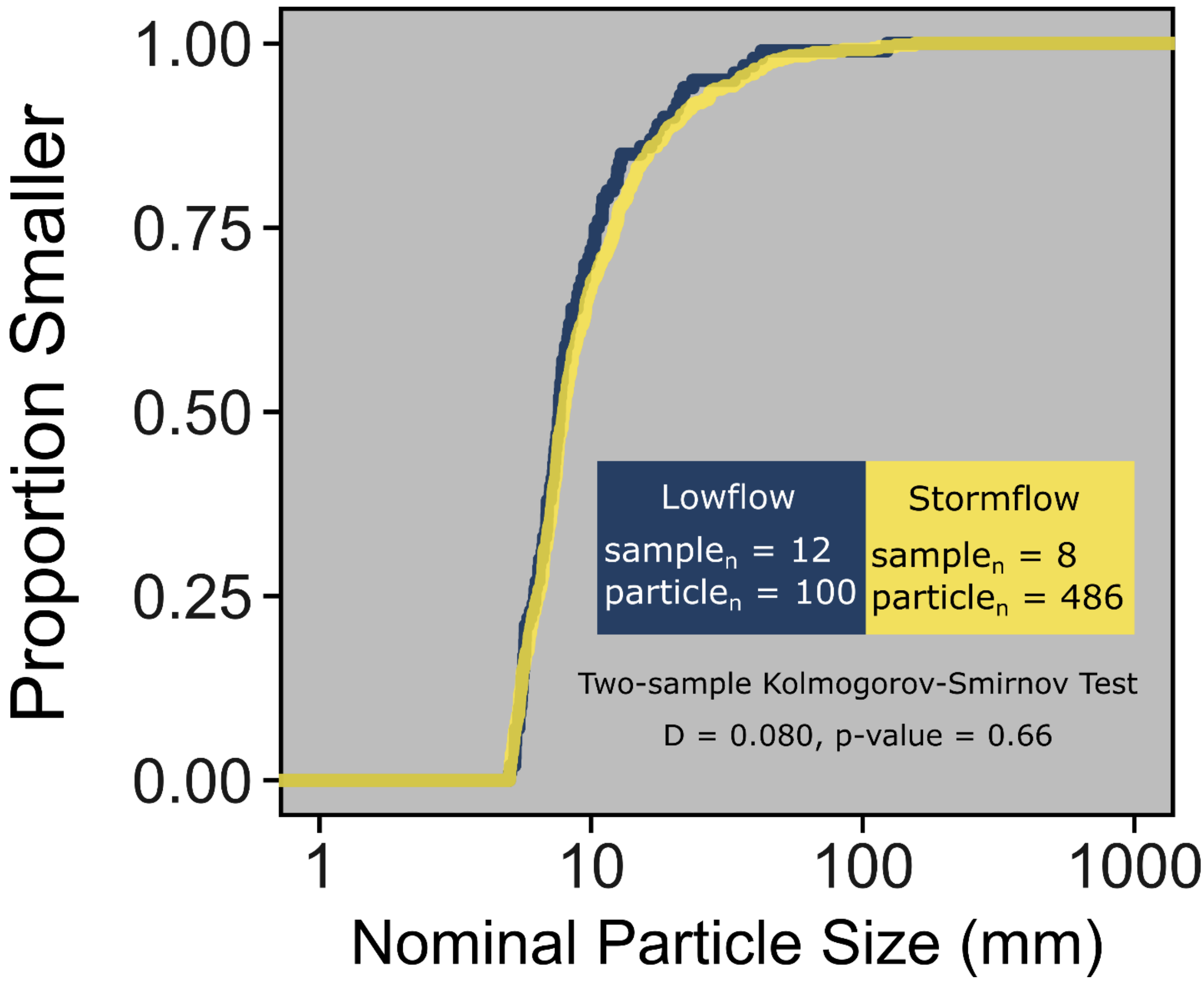

Figure 8: Empirical cumulative distribution functions for the nominal particle size (square root of particle projected surface area) of particles collected during stormflow and lowflow periods. $Particle_n$ refers to the total number of particles sampled during the respective transport mode. $Sample_n$ refers to the number of independent samples aggregated.

What can the observed uniform particle size distributions of macroplastic particles in riverflow tell us about watershed macroplastic pollution pathways and transport processes? The particle size distribution of macroplastics in riverflow is an expression of the macroplastic source's particle size distribution and the intervening channel's hydrologic transport characteristics. Large, positively buoyant particles only need a minimum water depth of ~ 25-50 % of their particle size to become mobilized (Braudrick and Grant, 2000). From a transportability perspective, it is unsurprising that we did not see a particle size preference because the river has an average depth of 0.16 m during lowflow conditions, which could mobilize the largest particle (0.4 m) that can fit in the opening of the net. From a source fingerprint perspective, the water at the site is nearly 100 % wastewater effluent during lowflow conditions. Macroplastic during these lowflow conditions can only be sourced from the channel. A predominant control of macroplastic particle size distributions during stormflow may occur in the river channel, or the particle size distribution of macroplastic outside the channel is the same as inside the channel. Future inquiry into particle size distributions of surface transportable macroplastic particles in the channel bed, riparian area, and watershed would help us better understand differences in the particle size distributions between regions. Other quantifiable macroplastic fingerprints like probability density functions of shapes, colors, and polymer type may also assist pathway description in future studies.

4.2 Hydrograph hysteresis and storm timing

We assessed the impact of hysteresis and storm timing on macroplastic concentration. Count concentrations ranged from 0.034 – 24 $num^1 m^{-3}$ and had a median concentration of 0.25 $num^{1}m^{-3}$ and a mean of 1.89 $num^{1}m^{-3}$. Mass concentrations ranged from 0.00047 – 2.99 $g^{1}m^{-3}$ and had a mean concentration of 0.22 $g^{1}m^{-3}$ and a median of 0.016 $g^{1}m^{-3}$. Macroplastic concentrations rose during the rising limb of one hydrograph (2019-2-2) and fell during the falling limb of another hydrograph (2019-1-17) (Figure 9). The same phenomenon was observed for mass concentrations (Figure 10). Assuming that macroplastic has stable hysteretic patterns, clockwise hysteresis would be the most likely explanation for this limited dataset, commonly also found for natural mineral sediment (Rose et al., 2018). Another macroplastic hydrograph sampling event in Northern California also observed clockwise hysteresis with macroplastic (5 Gyres and EOA inc., 2016) with the largest macroplastic concentration transporting during the very beginning of the stormflow. (Stenstrom and Kayhanian, 2005) also found that greater than 50% of litter flushes from roadsides in Southern California during the first 2 hr of stormflow. Clockwise hysteresis can be described from source mobilization and transport processes. We expect that floating macroplastic were always supply-limited since discharge conditions were always more than sufficient to effect transport, which could cause floating macroplastic supply to be rapidly depleted over the course of a stormflow. Another explanation can be provided by the transport rate of the floating macroplastic (which travel quickly at the river surface velocity) compared to the velocity of the peak of the discharge (which is much slower) (McDonnell and Beven, 2014), therefore one would expect the peak in macroplastic concentration to arrive before the discharge peak. Although hysteretic behavior can be stable at stream reaches (which would allow us to compare rising and falling limbs of different hydrographs), it has proven to be unstable for sediment in the Santa Ana river (Warrick and Rubin, 2007). A follow-up study is needed to collect data throughout a complete hydrograph on both sides of the peak discharge.

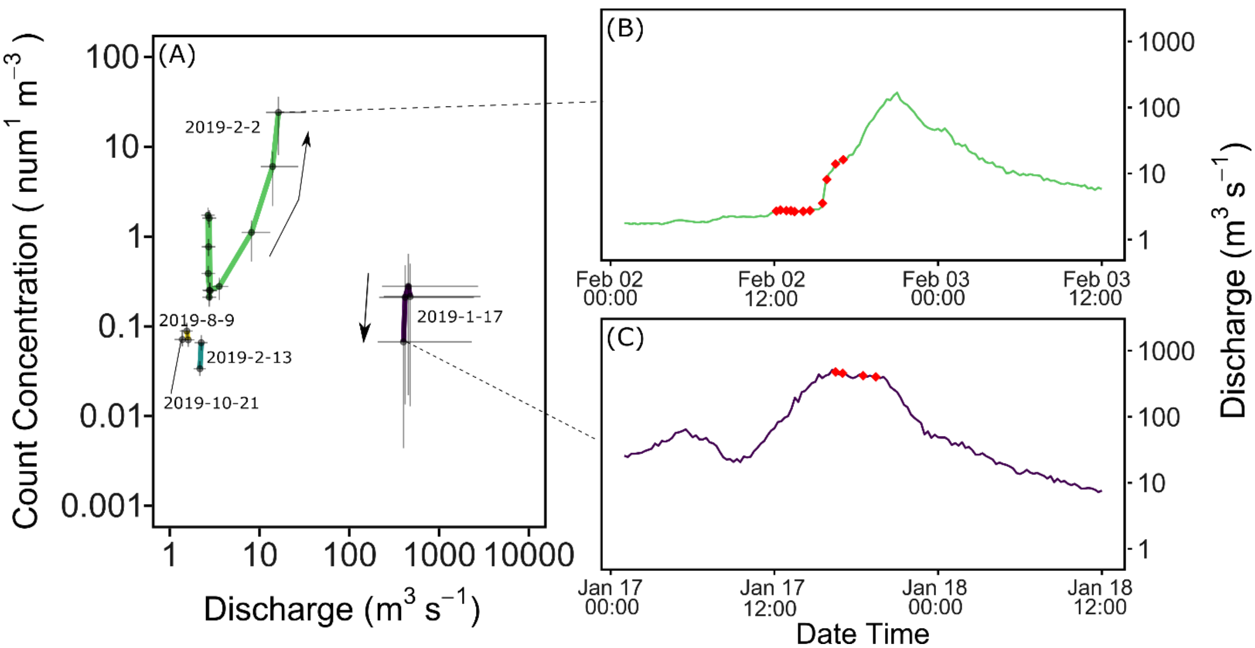

Figure 9: Concentration-discharge hysteresis for each sampling event. (A) Uncertainties from bootstrapped simulations are expressed as lines around the data points. Sampling events are uniquely colored, and hysteretic behavior is annotated using arrows to demonstrate the direction of the line during the sampling event. Dates are indicated nearest to each sampling event. The two storm hydrographs (B & C) are presented colored the same as the sampling event they are related to. Red dots are used to indicate the time and discharge when a sample was taken.

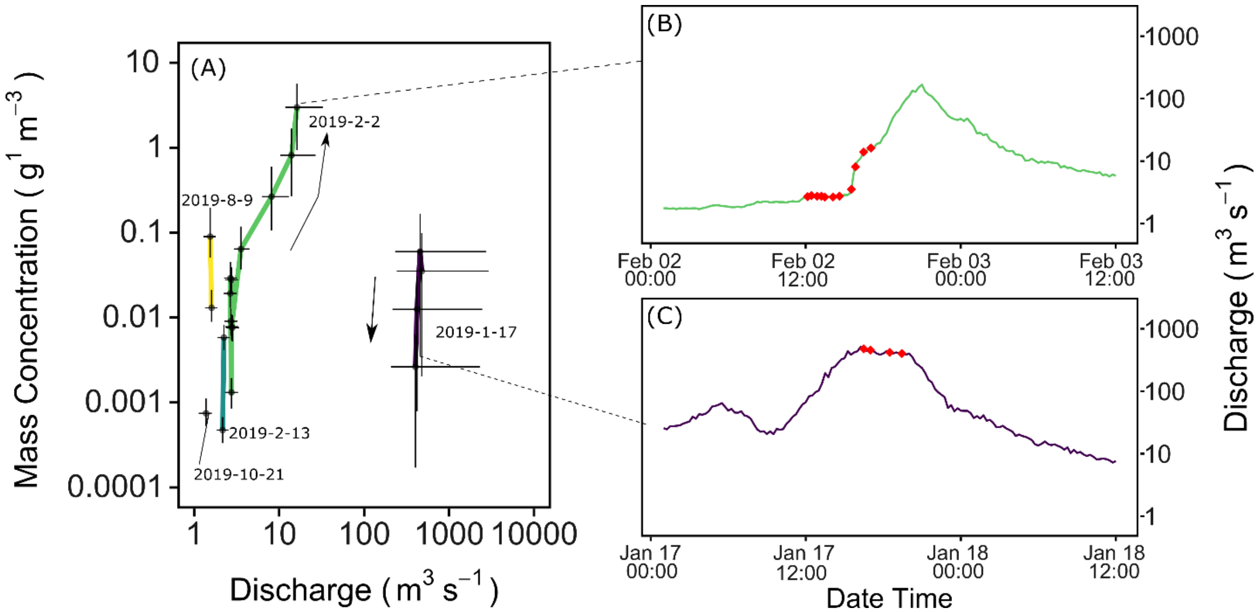

Figure 10: Mass concentration hysteresis analysis. (A) lines around the points indicate bootstrapped uncertainties. Each sampling day has its of color and a line connects the samples by time of sampling. An arrow indicates the direction the concentration line is going through time. (B) Hydrograph during February 2nd event with sample times plotted as red dots on the hydrograph. (C) Hydrograph during January 17th event with sample times plotted as red dots on the hydrograph.

A "first flush" event is common for many pollutants in Southern California, whereby high sediment concentrations are flushed during the first large storm event of the year. We found that an earlier storm event (1/17/2019) did not have higher concentrations than the later storm (2/2/2019). It is possible that we missed the first flush event since two stormflow events occurred before 1/17/2019 (Figure 4). It is also possible that the first flush event coincided with the 2/2/2019 event that we sampled. First flush events require a minimum storm magnitude threshold before they initiate (Kim et al., 2004). Future inquiry into first flush events for macroplastic should attempt to survey the first few hours of each stormflow of the year to standardize effects from hysteresis and better assess the role of storm timing (5 Gyres and EOA inc., 2016).

4.3 Macroplastic concentration-discharge rating curve

Our results show a statistically significant (p value < 0.05) rating curve between discharge and concentration ($\log_{10}$(count concentration) = s($\log_{10}$(discharge)) – 0.47, $\log_{10}$ correction = 1.19, DE = 67 %, n = 20, p value = 0.0002) (Figure 11). The same phenomenon was observed for mass concentrations (Figure 12). The rating curve was nonmonotonic, with the highest macroplastic concentration in the center of the observed discharges and the lowest concentrations at the highest and lowest discharges. As discharge increased, it could tap into additional sources of macroplastic at a rate of supply higher than that of water. However, water increased more rapidly than plastic at the highest discharges, resulting in lower concentrations. In the Santa Ana River, the flow covers a larger region of the channel corridor between levees during higher flows and can access all available macroplastics on the channel bed surface. Increases in discharge thereafter increase the flow depth in the channel, but do not access additional channel bed surface storage, which would result in a decrease in concentration if channel surface storage is an input location of buoyant plastic pollution in the sampled flows. The only other study of macroplastic concentration discharge relationships in Southern California (Moore et al., 2011) found generally higher concentrations by mass and count during wet weather flows but did not relate that to discharge magnitudes.

Interestingly, the concentration ranges observed for surface floating macroplastic in the Los Angeles river in 2004 by (Moore et al., 2011) (0 - 81 $g^{1}m^{-3}$, 0 – 18 $num^{1}m^{-3}$) overlaps with the concentration ranges observed in this study. A recent study also observed a similar nonmonotonic trend with increases at small increases in discharge and decreases in concentrations at the highest discharges (Haberstroh et al., 2021). However, concentration-discharge rating curves with a positive slope (5 Gyres and EOA inc., 2016), negative slope (van Emmerik et al., 2018), and no trend (Wagner et al., 2019) have been observed in other regions. At this time, we do not know what the primary driving force of variability is in concentration-discharge rating curves between watersheds.

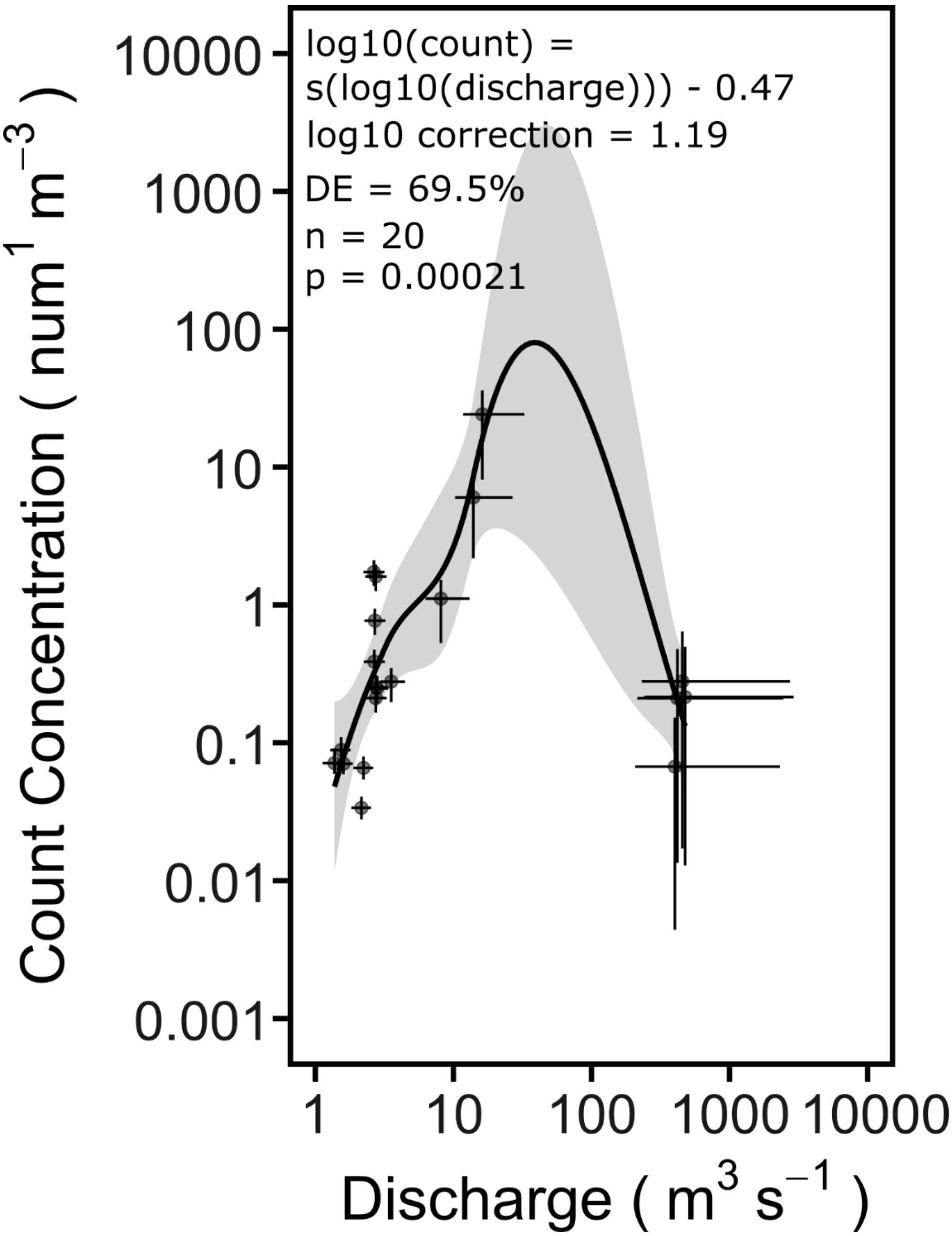

Figure 11: The generalized additive model on $\log_{10}$ transformed count concentration and discharge. In the top left corner, we provide the equation coefficients, number of observations, deviance explained, and p-value. Uncertainties for each data point's concentration and discharge values were bootstrapped and are provided as lines around each point.

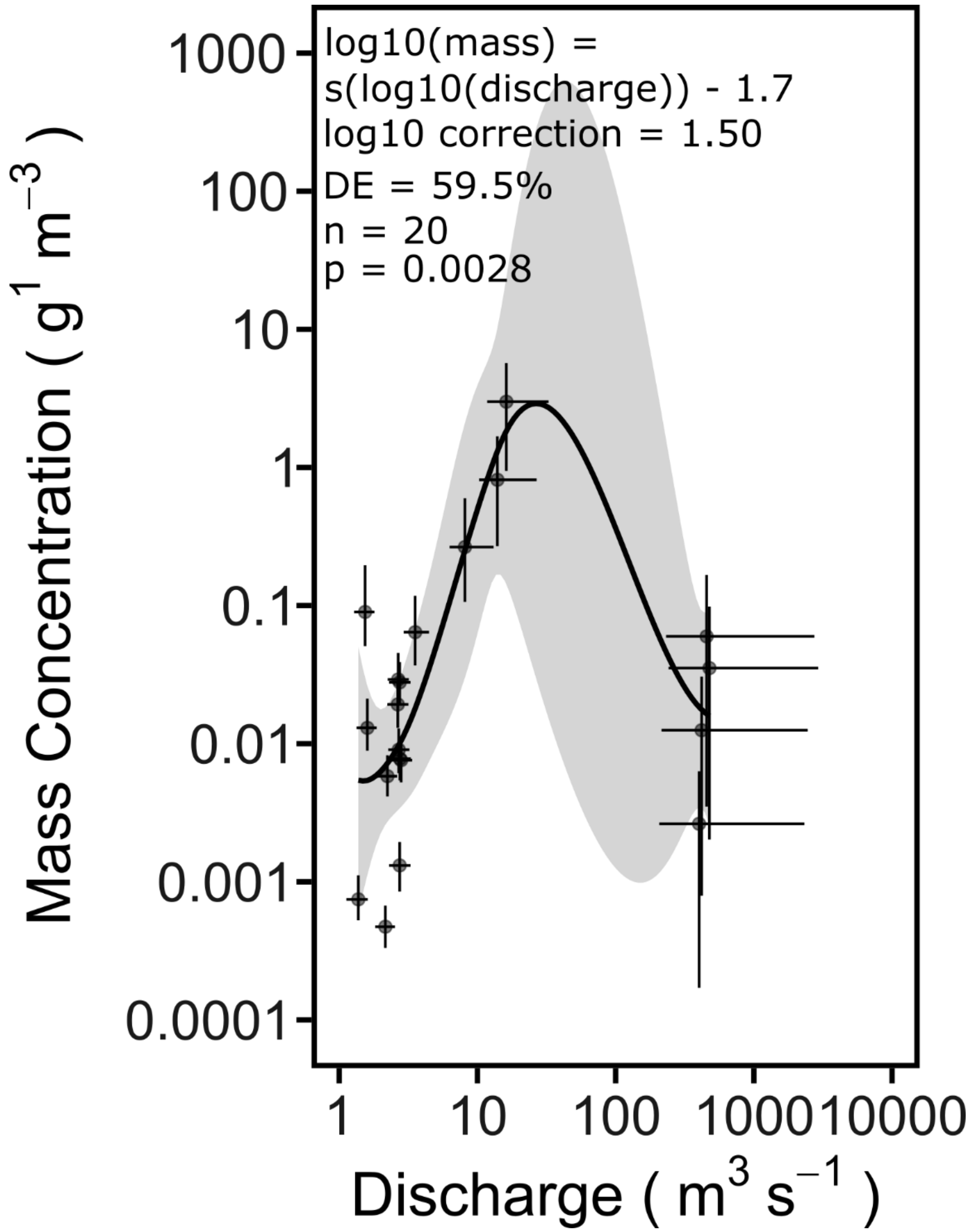

Figure 12: Generalized additive model using discharge to predict mass concentration. Deviance explained, sample size, and p-value for the smooth term are given. Uncertainties were bootstrapped around each observation and uncertainty range in discharge and concentration is given for each observation.

4.4 Estimating annual macroplastic flux

We used two flux estimation strategies to assess the impact of accounting for the concentration-discharge rating curves described in 3.3. The annual flux estimate based solely on mean concentration was 27 (2.82-84.8) metric tonnes and the concentration-discharge rating curve estimate (Figure 12) was 18.2 (2.9-222.2) metric tonnes (Figure 13). There is considerable overlap in the confidence intervals between the estimates. There was more uncertainty resulting from the concentration-discharge model fit because we introduced the uncertainty of the generalized additive model into the estimate. This underscores the importance of robust uncertainty assessment in flux estimation strategies, which can change the interpretation of the suitability differences between models. At this time, we would recommend using the mean concentration to estimate flux since it is a simpler model, but it likely underestimates uncertainty because systematic dependence on discharge and time is not included. More data is required to assess the differences between these estimates.

Future work should pursue the processes behind our preliminary findings of hydrograph hysteresis and nonmonotonic concentration-discharge relationships to decrease the uncertainty in those relationships for the Santa Ana River. The particle mass conversion from particle projected area could be improved by including morphological characteristics in the model or estimating particle density and the third dimension. Figure S2 shows particle size-to-mass relationships split up by particle morphologies. Some of the variability in the trend appears to be due to these morphological characteristics which likely correlate to both the third dimension and particle density. Studies investigating fluxes elsewhere should assess whether similar relationships exist and account for them in their flux estimates accordingly.

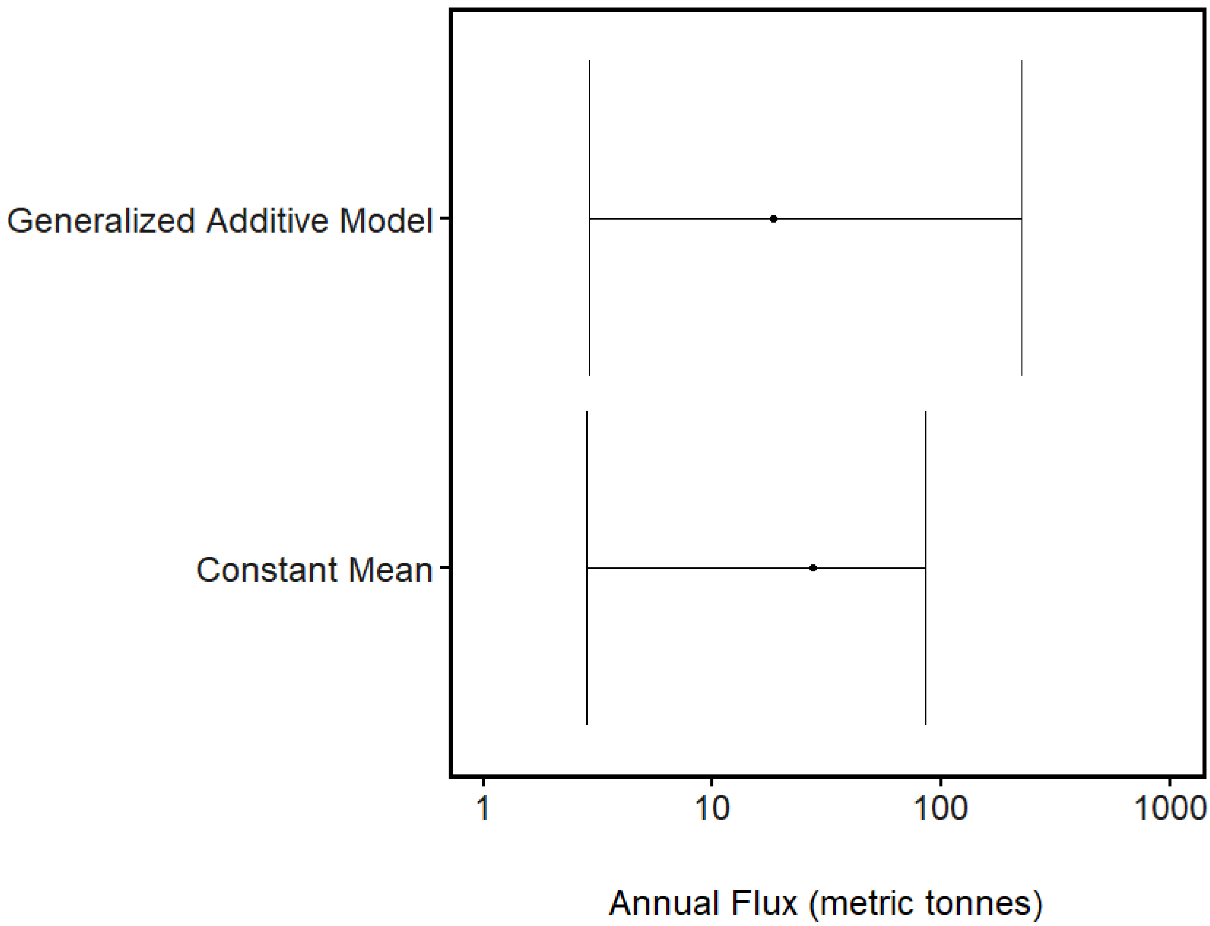

Figure 13: Total annual flux estimates (point) and uncertainties (whiskers) for estimating macroplastic flux using the Generalized Additive Model (18.2 (2.9-222.2) metric tonnes) (Figure 12) or the mean observed concentration (27 (2.82-84.8) metric tonnes).

5.0 Conclusions

This study was based on limited data (20 data points at one site) and should be considered as initial evidence toward a process-based understanding of macroplastic fate and transport processes in urban Southern California watersheds. Lowflow and stormflow samples had the same particle size distribution, suggesting that the channel is a critical location where particle size distributions are propagated or that the particle size distribution outside of the channel is the same as in the channel. Higher macroplastic concentrations were observed during the rising limb of a storm and lower concentrations observed during a near-peak falling limb, suggesting macroplastic source depletion early in storms or rapid mobility of macroplastic. However, future studies should measure macroplastic concentrations over the full range of a single hydrograph to avoid assuming that hysteresis is a stable process. Macroplastic concentrations were nonmonotonically related to discharge in terms of mass concentration and count concentration. Water year macroplastic flux estimates made using mean concentration and the concentration-discharge rating curve were not statistically distinguishable. Mean concentration may be appropriate to estimate flux when data availability is very low, but future studies should follow up on the findings revealed here to decrease uncertainty and further investigate the dependence of macroplastic concentration discharge relationships on time at the event to seasonal scale. A deeper analysis of sources and transport processes outside of the channel in the watershed would greatly advance our current understanding of how macroplastic is transported in this system. These phenomena may be particularly important in small, mountainous semi-arid systems such as the Santa Ana River where in-channel storage of macroplastics may be particularly high, and the readily mobilized by flashy stormflow regimes.

Funding

W. Cowger was funded in part by an NSF Graduate Research Fellowship. This project was supported in part by the USDA National Institute of Food and Agriculture, Hatch program [project number CA-R-ENS-5120-H], USDA Multistate Project 4170 [project number CA-R-ENS-5189-RR], the UC ANR AES Mission Funding Program, and NOAA Marine Debris Research grant #NA19NOS9990086. K. Waldschläger was supported by the Investment Plan for strengthening the Technical Sciences at Wageningen University.

Acknowledgments

We thank Shannon Tarby, Trevor Lok, Nathan Jumps, and Julianna McDonnell for helping with field and lab work. We thank Marcus Eriksen of 5 Gyres for initial conversations on sampling approaches and for providing the sampling device.

Research Data

New data and code created in this manuscript are shared open access on Open Science Framework (DOI 10.17605/OSF.IO/MREY8) to ensure the reproducibility and comparability of this research.

References

5 Gyres and EOA inc., 2016. Testing Trash “Flux” Monitoring Methods in Flowing Water Bodies.

Aguilera, R., Melack, J.M., 2018. Concentration-Discharge Responses to Storm Events in Coastal California Watersheds. Water Resour. Res. 54, 407–424.

Bai, M., Lin, Y., Hurley, R.R., Zhu, L., Li, D., 2021. Controlling Factors of Microplastic Riverine Flux and Implications for Reliable Monitoring Strategy. Environmental Science & Technology. https://doi.org/10.1021/acs.est.1c04957

Bengtsson, H., 2021. matrixStats: Functions that Apply to Rows and Columns of Matrices (and to Vectors).

Braudrick, C.A., Grant, G.E., 2000. When do logs move in rivers? Water Resour. Res. 36, 571–583.

Cowger, W., Booth, A.M., Hamilton, B.M., Thaysen, C., Primpke, S., Munno, K., Lusher, A.L., Dehaut, A., Vaz, V.P., Liboiron, M., Devriese, L.I., Hermabessiere, L., Rochman, C., Athey, S.N., Lynch, J.M., De Frond, H., Gray, A., Jones, O.A.H., Brander, S., Steele, C., Moore, S., Sanchez, A., Nel, H., 2020. Reporting Guidelines to Increase the Reproducibility and Comparability of Research on Microplastics. Applied Spectroscopy 74. https://doi.org/10.1177/0003702820930292

Cowger, W., Gray, A., Hapich, H., Osei-Enin, J., Olguin, S., Huynh, B., Nogi, H., Singh, S., Brownlee, S., Fong, J., Lok, T., Singer, G., Ajami, H., 2022. Litter origins, accumulation rates, and hierarchical composition on urban roadsides of the Inland Empire, California. Environmental Research Letters 17, 15007. https://doi.org/10.1088/1748-9326/ac3c6a

Cowger, W., Gray, A.B., Guilinger, J.J., Fong, B., Waldschläger, K., 2021a. Concentration Depth Profiles of Microplastic Particles in River Flow and Implications for Surface Sampling. Environ. Sci. Technol. 55, 6032–6041. https://doi.org/10.1021/acs.est.1c01768

Cowger, W., Gray, A.B., Schultz, R.C., 2019. Anthropogenic litter cleanups in Iowa riparian areas reveal the importance of near-stream and watershed scale land use. Environmental Pollution 250, 981–989. https://doi.org/10.1016/j.envpol.2019.04.052

Cowger, W., Steinmetz, Z., Gray, A., Munno, K., Lynch, J., Hapich, H., Primpke, S., De Frond, H., Rochman, C., Herodotou, O., 2021b. Microplastic Spectral Classification Needs an Open Source Community: Open Specy to the Rescue! Anal. Chem. 93, 7543–7548.

De Cicco, L.A., Lorenz, D., Hirsch, R.M., Watkins, W., Johnson, M., 2021. dataRetrieval: R packages for discovering and retrieving water data available from U.S. federal hydrologic web services. https://doi.org/10.5066/P9X4L3GE

de Leeuw, J., Lamb, M.P., Parker, G., Moodie, A.J., Haught, D., Venditti, J.G., Nittrouer, J.A., 2020. Entrainment and suspension of sand and gravel. Earth Surf. Dynam. 8, 485–504. https://doi.org/10.5194/esurf-8-485-2020

Dowle, M., Srinivasan, A., 2020. data.table: Extension of \`data.frame\`.

East, A.E., Stevens, A.W., Ritchie, A.C., Barnard, P.L., Campbell-Swarzenski, P., Collins, B.D., Conaway, C.H., 2018. A regime shift in sediment export from a coastal watershed during a record wet winter, California: Implications for landscape response to hydroclimatic extremes. Earth Surface Processes and Landforms 43, 2562–2577. https://doi.org/10.1002/esp.4415

Farnsworth, K.L., Milliman, J.D., 2003. Effects of climatic and anthropogenic change on small mountainous rivers: the Salinas River example. Global and Planetary Change 39, 53–64. https://doi.org/10.1016/S0921-8181(03)00017-1

Ferguson, R.I., 1986. River Loads Underestimated by Rating Curves. Water Resources Research 22, 74–76. https://doi.org/10.1029/WR022i001p00074

Fisher, A., Belmont, P., Murphy, B.P., MacDonald, L., Ferrier, K.L., Hu, K., 2021. Natural and anthropogenic controls on sediment rating curves in northern California coastal watersheds. Earth Surface Processes and Landforms 46, 1610–1628. https://doi.org/10.1002/esp.5137

Garnier, S., 2018. viridis: Default Color Maps from “matplotlib.”

Gray, A.B., 2018. The impact of persistent dynamics on suspended sediment load estimation. Geomorphology 322, 132–147. https://doi.org/10.1016/j.geomorph.2018.09.001

Gray, A.B., Pasternack, G.B., Watson, E.B., Warrick, J.A., Goñi, M.A., 2015. Effects of antecedent hydrologic conditions, time dependence, and climate cycles on the suspended sediment load of the Salinas River, California. Journal of Hydrology 525, 632–649. https://doi.org/10.1016/j.jhydrol.2015.04.025

Gray, A.B., Warrick, J.A., Pasternack, G.B., Watson, E.B., Goñi, M.A., 2014. Suspended sediment behavior in a coastal dry-summer subtropical catchment: Effects of hydrologic preconditions. Geomorphology 214, 485–501. https://doi.org/10.1016/j.geomorph.2014.03.009

Haberstroh, C.J., Arias, M.E., Yin, Z., Wang, M.C., 2021. Effects of Urban Hydrology on Plastic Transport in a Subtropical River. ACS ES&T Water 1, 1714–1727. https://doi.org/10.1021/acsestwater.1c00072

Kim, L.-H., Kayhanian, M., Stenstrom, M.K., 2004. Event mean concentration and loading of litter from highways during storms. Sci. Total Environ. 330, 101–113.

Kooi, M., Koelmans, A.A., 2019. Simplifying microplastic via continuous probability distributions for size, shape, and density. Environmental Science & Technology Letters 6, 551–557.

Kroon, F., Motti, C., Talbot, S., Sobral, P., Puotinen, M., 2018. A workflow for improving estimates of microplastic contamination in marine waters: A case study from {North-Western} Australia. Environ. Pollut. 238, 26–38.

L. Lebreton, B. Slat, F. Ferrari, B. Sainte-Rose, J. Aitken, R. Marthouse, S. Hajbane, S. Cunsolo, A. Schwarz, A. Levivier, K. Noble, P. Debeljak, H. Maral, R. Schoeneich-Argent, R. Brambini & J. Reisser, 2018. Evidence that the Great Pacific Garbage Patch is rapidly accumulating plastic. Sci. Rep. 8.

Lebreton, L.C.M., van der Zwet, J., Damsteeg, J.-W., Slat, B., Andrady, A., Reisser, J., 2017. River plastic emissions to the world's oceans. Nat. Commun. 8, ncomms15611.

Li Yingxia, Lau Sim-Lin, Kayhanian Masoud, Stenstrom Michael K., 2005. Particle Size Distribution in Highway Runoff. J. Environ. Eng. 131, 1267–1276.

McDonnell, J.J., Beven, K., 2014. Debates-The future of hydrological sciences: A (common) path forward? A call to action aimed at understanding velocities, celerities and residence time distributions of the headwater hydrograph. Water Resources Research 50, 5342–5350. https://doi.org/10.1002/2013WR015141

Midwestern Regional Climate Center, 2021. cli-MATE [WWW Document]. URL https://mrcc.purdue.edu/CLIMATE/

Moore, C.J., Lattin, G.L., Zellers, A.F., 2011. Quantity and type of plastic debris flowing from two urban rivers to coastal waters and beaches of Southern California. Revista de Gestão Costeira Integrada 11, 65–73.

Moore, S., Sutula, M., Von Bitner, T., Lattin, G., Schiff, K., 2016. Southern California Bight 20 Regional Monitoring Program: Volume {III}. Trash and Marine Debris.

Muthuvairavasamy, R., 2022. Types and Classifiction of Plastic Pollutants, in: Muthuvairavasamy, R. (Ed.), Microplastics: Footprints On The Earth and Their Environmental Management. Springer International Publishing, Cham, pp. 7–18. https://doi.org/10.1007/978-3-031-10729-0_2

National Inventory of Dams [WWW Document], 2018. . FEMA. URL https://www.fema.gov/emergency-managers/risk-management/dam-safety/national-inventory-dams (accessed 8.29.22).

Riverside City, 2021. Street Sweeping Program [WWW Document]. URL https://riversideca.gov/streets/street-sweeping.asp

Riverside County, 2010. NATIONAL POLLUTANT DISCHARGE ELIMINATION SYSTEM (NPDES) PERMIT AND WASTE DISCHARGE REQUIREMENTS FOR THE RIVERSIDE COUNTY FLOOD CONTROL AND WATER CONSERVATION DISTRICT, THE COUNTY OF RIVERSIDE.

Rose, L.A., Karwan, D.L., Godsey, S.E., 2018. Concentration-discharge relationships describe solute and sediment mobilization, reaction, and transport at event and longer timescales. Hydrol. Process. 32, 2829–2844.

Sansalone John J., Cristina Chad M., 2004. First Flush Concepts for Suspended and Dissolved Solids in Small Impervious Watersheds. J. Environ. Eng. 130, 1301–1314.

Schindelin, J., Arganda-Carreras, I., Frise, E., Kaynig, V., Longair, M., Pietzsch, T., Preibisch, S., Rueden, C., Saalfeld, S., Schmid, B., Tinevez, J.-Y., White, D.J., Hartenstein, V., Eliceiri, K., Tomancak, P., Cardona, A., 2012. Fiji: an open-source platform for biological-image analysis. Nature Methods 9, 676–682. https://doi.org/10.1038/nmeth.2019

Schmidt, C., Krauth, T., Wagner, S., 2017. Export of Plastic Debris by Rivers into the Sea. Environmental Science & Technology 51, 12246–12253. https://doi.org/10.1021/acs.est.7b02368

Slattery, M.C., Burt, T.P., 1997. Particle size characteristics of suspended sediment in hillslope runoff and stream flow. Earth Surface Processes and Landforms: The Journal of the British Geomorphological Group 22, 705–719.

Stenstrom, M.K., Kayhanian, M., 2005. First Flush Phenomenon Characterization. Caltrans.

USGS, 2019. National Hydrography Dataset [WWW Document]. URL https://search.library.wisc.edu/catalog/9910061259502121

USGS, 2017. 1/9th Arc-second Digital Elevation Models (DEMs) - USGS National Map 3DEP Downloadable Data Collection: U.S. Geological Survey [WWW Document]. URL https://www.sciencebase.gov/catalog/item/4f70aac4e4b058caae3f8de7

USGS, 2016a. StreamStats [WWW Document]. URL http://streamstats.usgs.gov/

USGS, 2016b. National Water Information System data available on the World Wide Web (USGS Water Data for the Nation) [WWW Document]. http://dx.doi.org/10.5066/F7P55KJN

van Emmerik, T., 2021. Macroplastic research in an era of microplastic. Microplastics and Nanoplastics 1, 1–2.

van Emmerik, T., Kieu-Le, T.-C., Loozen, M., van Oeveren, K., Strady, E., Bui, X.-T., Egger, M., Gasperi, J., Lebreton, L., Nguyen, P.-D., Schwarz, A., Slat, B., Tassin, B., 2018. A Methodology to Characterize Riverine Macroplastic Emission Into the Ocean. Frontiers in Marine Science 5, 372.

Van Emmerik, T., Loozen, M., Van Oeveren, K., Buschman, F., Prinsen, G., 2019. Riverine plastic emission from Jakarta into the ocean. Environ. Res. Lett. 14, 84033.

van Emmerik, T., Tramoy, R., van Calcar, C., Alligant, S., Treilles, R., Tassin, B., Gasperi, J., 2019. Seine Plastic Debris Transport Tenfolded During Increased River Discharge. Frontiers in Marine Science 6, 642.

Venables, W.N., Ripley, B.D., 2002. Modern Applied Statistics with S, Fourth. ed. Springer, New York.

Wagner, S., Klöckner, P., Stier, B., Römer, M., Seiwert, B., Reemtsma, T., Schmidt, C., 2019. Relationship between Discharge and River Plastic Concentrations in a Rural and an Urban Catchment. Environmental Science & Technology 53, 10082–10091. https://doi.org/10.1021/acs.est.9b03048

Waldschläger, K., Born, M., Cowger, W., Gray, A., Schüttrumpf, H., 2020. Settling and rising velocities of environmentally weathered micro- and macroplastic particles. Environmental Research 191. https://doi.org/10.1016/j.envres.2020.110192

Waldschläger, K., Brückner, M.Z.M., Carney Almroth, B., Hackney, C.R., Adyel, T.M., Alimi, O.S., Belontz, S.L., Cowger, W., Doyle, D., Gray, A., Kane, I., Kooi, M., Kramer, M., Lechthaler, S., Michie, L., Nordam, T., Pohl, F., Russell, C., Thit, A., Umar, W., Valero, D., Varrani, A., Warrier, A.K., Woodall, L.C., Wu, N., 2022. Learning from natural sediments to tackle microplastics challenges: A multidisciplinary perspective. Earth-Science Reviews 228, 104021. https://doi.org/10.1016/j.earscirev.2022.104021

Walling, D.E., 1977. Assessing the accuracy of suspended sediment rating curves for a small basin. Water Resour. Res. 13, 531–538.

Warrick, J.A., Madej, M.A., Goñi, M.A., Wheatcroft, R.A., 2013. Trends in the suspended-sediment yields of coastal rivers of northern California, 1955–2010. Journal of Hydrology 489, 108–123. https://doi.org/10.1016/j.jhydrol.2013.02.041

Warrick, J.A., Rubin, D.M., 2007. Suspended-sediment rating curve response to urbanization and wildfire, Santa Ana River, California. J. Geophys. Res. 112, F02018.

Watkins, L., Sullivan, P.J., Walter, M.T., 2019. A case study investigating temporal factors that influence microplastic concentration in streams under different treatment regimes. Environmental Science and Pollution Research 26, 21797–21807. https://doi.org/10.1007/s11356-019-04663-8

Wickham, H., 2019. stringr: Simple, Consistent Wrappers for Common String Operations.

Wickham, H., 2016. ggplot2: elegant graphics for data analysis.

Wickham, H., Bryan, J., 2019. readxl: Read Excel Files.

Wickham, H., François, R., Henry, L., Müller, K., 2020. dplyr: A Grammar of Data Manipulation.

Wickham, H., Henry, L., 2020. tidyr: Tidy Messy Data.

Williams, G.P., Others, 1989. Sediment concentration versus water discharge during single hydrologic events in rivers. J. Hydrol. 111, 89–106.

Wood, S.N., 2011. Fast stable restricted maximum likelihood and marginal likelihood estimation of semiparametric generalized linear models. Journal of the Royal Statistical Society (B) 73, 3–36.